Structure and Energetics of an Allele-Specific Genetic Interaction between *dnaJ* and *dnaK*: Correlation of Nuclear Magnetic Resonance Chemical Shift Perturbations in the J-Domain of Hsp40/DnaJ with Binding Affinity for the ATPase Domain of Hsp70/DnaK†

Samuel J. Landry*

Department of Biochemistry, Tulane University Health Sciences Center, New Orleans, Louisiana 70112

Received October 28, 2002; Revised Manuscript Received March 11, 2003

ABSTRACT: The molecular chaperone machine composed of *Escherichia coli* Hsp70/DnaK and Hsp40/DnaJ binds and releases client proteins in cycles of ATP-dependent protein folding, membrane translocation, disassembly, and degradation. The J-domain of DnaJ simultaneously stimulates ATP hydrolysis in the ATPase domain and capture of the client protein in the peptide-binding domain of DnaK. ATP-dependent binding of DnaJ to DnaK mimics DnaJ-dependent capture of a client protein. The *dnaJ* mutation that replaces aspartate-35 with asparagine (D35N) in the J-domain causes a defect in binding of DnaJ to DnaK. The *dnaK* mutation that replaces arginine-167 with alanine (R167A) in the ATPase domain of DnaK-(R167A) restores binding of DnaJ(D35N). This genetic interaction was said to be allele-specific because wild-type DnaJ does not bind to DnaK(R167A). The J-domain of DnaJ binds to the ATPase domain of DnaK in its capacity as modulator of DnaK ATPase activity and conformational behavior. Surprisingly, the mutations affect the domainwise interaction in an almost opposite manner. D35N increases the affinity of the J-domain for the ATPase domain. R167A has no affect on the affinity of the ATPase domain for the D35N mutant J-domain, but it reduces the affinity for the wild-type J-domain. Previous amide (^{1}H, ^{15}N) NMR chemical shift perturbation mapping in the J-domain suggested that the ATPase domain binds to J-domain helix II and the flanking loops. In the D35N mutant J-domain, chemical shift perturbations include additional effects at amides in the flexible loop II−III and helix III, which have been proposed to undergo an induced fit conformational change upon binding to DnaK. The integrated magnitudes of chemical shift perturbations for the various J-domain and ATPase domain pairs correlate with the free energies of binding. Thus, the J-domain structure can be described as a dynamic ensemble of conformations that is constrained by binding to the ATPase domain. J-domain helix II bends upon binding to the ATPase domain. D35N increases helix II bending, but less so in combination with R167A in the ATPase domain. Taken together, the results suggest that D35N overstabilizes an induced fit conformational change in loop II−III and helix III that is necessary for the J-domain to couple ATP hydrolysis with a conformational change in DnaK, and R167A destabilizes the induced conformation. Conclusions from this work have implications for understanding mechanisms of protein−protein interaction that are involved in allosteric regulation and genetic suppression.

Hsp70[1] uses ATP hydrolysis to switch between states of low and high affinity for client proteins (*1*, *2*). Hsp40 stimulates ATP hydrolysis by Hsp70 (*3*), targets client proteins for Hsp70 binding (*4*, *5*), and couples ATP hydrolysis to the work of protein folding (*6*). Some Hsp40-like proteins, such as those induced by heat shock, probably have low specificity for client proteins, whereas other Hsp40-like proteins may be dedicated to particular clients, such as auxilin for clathrin cages (*7*) and Hsc20 for the IscU Fe/S assembly protein (*8*). All Hsp40-like proteins are distinguished by the presence of a 75-residue J-domain that enables them to catalyze loading of client proteins onto Hsp70s (*4*, *9*).

Mechanisms of interdomain communication in Hsp70 remain to be defined. There is no structure available for either a full-length Hsp70 or a complex of individual domains. Crystal structures are available for the ATPase domains from mammalian Hsc70 (*10*) and *Escherichia coli* DnaK (*11*). The ATPase domain closes around the nucleotide, but it is unclear how it communicates with the C-terminal peptide-binding domain. A crystal structure for the DnaK peptide-binding domain reveals an all-β subdomain that encloses peptides with protruding loops and an all-α subdomain that forms a "lid" over the peptide-binding site (*12*). The DnaK ATPase activity modulates access of peptides to the peptide-binding

† The author acknowledges support from the Tulane University Wall Fund, the Louisiana Board of Regents [LEQSF(2001−2002) ENH-TR70], and the National Science Foundation (CTS-9977269).

* To whom correspondence should be addressed: (504) 586-3990 (phone); (504) 584-2739 (fax); landry@tulane.edu (e-mail).

[1] Abbreviations: Hsp70, 70 kDa heat shock protein; Hsp40, 40 kDa heat shock protein; Jd, recombinant J-domain of *Escherichia coli* DnaJ; JdD35N, recombinant D35N mutant J-domain; Jdp5, recombinant protein composed of the J-domain and peptide p5; JdD35Np5, recombinant protein composed of the D35N mutant J-domain and peptide p5; Kase, recombinant ATPase domain of *E. coli* DnaK; ITC, isothermal titration calorimetry.

10.1021/bi027070y CCC: $25.00 © 2003 American Chemical Society
Published on Web 04/11/2003

domain (*13*), and conversely, peptides stimulate the ATPase (*14*). Several laboratories have identified residues in various Hsp70s that affect coupling between ATPase and peptide-binding domains (*15*−*21*).

The modular architecture of Hsp40-like proteins suggests that they adapt substrates for Hsp70 binding. Usually the J-domain is N-terminal, as in DnaJ. However, the J-domain is C-terminal in auxilin, and it lies between membrane-spanning segments in the ER translocation factor, Sec63 (*22*). Sequence alignment of DnaJ homologues identified at least three domains following the J-domain, all of which may be involved in substrate binding. These are the Gly/Phe-rich region, the Zn^{2+}-binding region, and a C-terminal region (*22*).

Three-dimensional structures of J-domains from *E. coli* DnaJ (*23*, *24*), human Hdj1 (*25*), *E. coli* Hsc20 (*26*), polyomavirus T-antigen (*27*), and simian virus 40 T-antigen (*28*) reveal a common fold composed of four α helices. The central helices II and III form a coiled coil, and the intervening loop II−III contains the J-domain signature sequence, histidine−proline−aspartate (HPD). A number of mutations in the J-domain have been shown to disrupt binding of J-domain proteins to Hsp70s (*16*, *29*−*31*). A previous NMR signal perturbation mapping study showed that the binding site for DnaK on a recombinant J-domain (Jd) is centered on helix II and extends over the adjacent HPD tripeptide, and it showed that the DnaK ATPase domain contains the J-domain-binding site (*32*).

Dissection of an allele-specific genetic interaction between the *dnaK* and *dnaJ* should reveal important aspects of J-domain function. A defective phenotype caused by a mutation encoding D35N in the J-domain of DnaJ was partially reversed by suppressor mutations encoding R167H or R167A in the ATPase domain of DnaK (*16*). This genetic interaction was explained by DnaJ−DnaK interactions in vitro. DnaJ(D35N) was defective for ATP-dependent binding to DnaK but was competent for binding to DnaK(R167H/A). The interaction was said to be allele-specific because DnaJ was defective for binding to DnaK(R167H/A). Gross and co-workers considered the possibility that D35 directly contacted R167 across the DnaJ−DnaK binding interface but ultimately concluded that histidine and alanine were not sufficiently similar to support this mechanism of suppression.

Recently, we have shown that Jd can simultaneously stimulate ATP hydrolysis and conversion of DnaK into the conformation with high affinity for peptides (*33*). The mutant J-domain (JdD35N) was unable to stimulate ATP hydrolysis or the conformational change, despite the fact that it bound to DnaK with greater than wild-type affinity. Experiments with fusion proteins composed of wild-type or mutant J-domain and a DnaK-binding peptide suggest that the J-domain accelerates ATP hydrolysis and delays the DnaK conformational change in order to couple the two processes. The mutant J-domain appears to be completely defective in stimulating ATP hydrolysis, but it can block the DnaK conformational change.

Amide group NMR chemical shifts provide detailed information about local structure in proteins. Chemical shift dispersion arises from local positive shielding induced by the magnetic field in electron clouds surrounding the resonant nucleus. Interatomic shielding augments or opposes the local positive shielding, depending on the type and orientation of bonds and the presence of electron-withdrawing groups. Ring currents of aromatic side chains exert an especially strong interatomic shielding effect whose direction depends on the position of the nucleus relative to the plane of the ring. With the availability of high-resolution structural information, the chemical shifts of amide and C_α protons in proteins can be predicted with good precision. After taking into account the random-coil chemical shifts for each amino acid and ring-current shifts, the dominant single factor determining the chemical shift of amide protons is the length of the local H-bond (*34*, *35*). Several features of protein structure determine the chemical shift of amide nitrogens, including the local secondary structure, type of side chain in the neighboring residues, and hydrogen bonding (*36*).

The sensitivity of chemical shifts to local structural features provides an excellent tool for analyzing protein−protein interactions. Several protein−protein binding sites that were mapped by amide ^1H and ^{15}N chemical shift perturbations have been corroborated by high-resolution crystal structures (*37*−*39*). Investigators rarely discuss the local structural effects that cause chemical shift perturbations, but the perturbations presumably are caused by changes in ring-current shifts and from the strengthening or weakening of hydrogen bonds.

The extent and character of a binding interface are the most important parameters determining binding affinity and specificity, and almost all studies using NMR chemical shift perturbation discuss these features of the interface (*40*). Some also discuss perturbations outside of the putative interface as indicators of conformational change associated with binding (*41*−*44*). Only a few studies have compared perturbation patterns produced by different binding partners or compared patterns produced by the same partners in different conditions (*45*−*47*), and they have focused on qualitative differences in the interfaces.

Here, amide ^1H and ^{15}N chemical shift perturbation experiments show that D35N alters the mode of J-domain binding to the DnaK ATPase domain. For the set of four wild-type and mutant pairs of the J-domain (Jd and JdD35N) and ATPase domain (Kase and KaseR167A), the integrated chemical shift perturbations for all observed amides correlate with the binding affinity. Thus, changes in chemical shift perturbations indicate changes in the contribution to the binding affinity of structural features in the Jd-Kase interface. D35N most likely overstabilizes an induced fit conformational change in loop II−III and helix III of the J-domain, and R167A destabilizes the induced conformation. Details of the binding interaction appear to have a profound effect on the catalytic action of the J-domain on DnaK.

MATERIALS AND METHODS

Proteins. The sequence encoding Kase (DnaK residues 2−388) in pRLM157 (generously provided by R. McMacken) was modified to encode the R167A substitution using appropriate oligonucleotides and the QuickChange site-directed mutagenesis kit (Stratagene). Jd (DnaJ residues 2−75) and JdD35N were prepared as described (*33*). [^{15}N]Jd and [^{15}N]JdD35N were expressed in *E. coli* Nap IV cells and purified using the protocol described previously for wild-type [^{15}N]Jd (*32*), with the sole modification that dithiothreitol and glycerol were omitted from buffer solutions. Purification of Kase and KaseR167A was as described for

DnaK (*14*). Protein concentrations were determined by the Bio-Rad protein assay and verified by quantitative amino acid analysis.

Circular Dichroism and Thermal Denaturation. Far-ultraviolet circular dichroism (CD) experiments were performed on a Jasco 810 CD spectropolarimeter with the bandwidth set to 2 nm. Samples contained 4 μM protein and 5 mM sodium phosphate buffer, pH 6.8. The path length was 0.1 cm. Triplicate wavelength scans were recorded over the range of 186−260 nm in 2 nm steps with a response time of 2 s, averaged together, and then the corresponding spectrum of buffer only was subtracted. Thermal denaturation was monitored at 222 nm using a response time of 4 s as the temperature was increased from 10 to 90 °C in steps of 1 °C min^{-1}. The thermal unfolding curve for each protein was fit by nonlinear regression (GraphPad Prism) to the equation:

$$y = \{(y_f + m_f[T]) + (y_u + m_u[T])\exp[(\Delta H_m/RT)((T - T_m)/T_m)]\}/(1 + \exp[(\Delta H_m/RT)((T - T_m)/T_m)])$$

where y represents the observed CD signal, y_f and y_u are the intercepts and m_f and m_u are the slopes of the pre- and posttransition baselines, T is the temperature, T_m is the midpoint of the thermal unfolding curve, and ΔH_m is the enthalpy change for unfolding at T_m (*48*).

Calorimetry. Calorimetric titrations were performed with a VP-ITC (MicroCal). Jd or JdD35N (1.15 mM) was injected in 10 μL increments into a solution of KaseR167A (initially 0.048 mM) at 20 °C. Dialysis of the proteins together in the same buffer solution [50 mM morpholinoethanesulfonic acid (MOPS)−NaOH, pH 6.7] minimized uncertainty in the comparison of thermodynamic quantities. Chilled protein samples were degassed under house vacuum prior to being loaded. The reference power was set to 10 μcal s^{-1}. Baseline heats of dilution (corresponding to approximately 240 cal/mol of complex) determined by injecting Jd or JdD35N into buffer were not appropriate for subtraction from actual experiments with KaseR167A. Instead, the baseline heat of dilution was treated as a variable in fitting each curve of ΔH vs protein ratio using the facility in MicroCal Origin. Optimum values of X^2 were obtained for baselines ranging from 170 to 200 cal/mol of complex.

NMR. Samples were prepared initially in 550 μL of 50 mM MOPS−NaOH, pH 6.7, and then 48 μL of D_2O and 1.2 μL of 80 mM NaN_3 were added. The final concentration of [^{15}N]Jd or [^{15}N]JdD35N prior to addition of the ATP domain was 40 μM. Kase or KaseR167A was added in increments of 2.5−25 μL. Final concentrations of Kase were 0, 9.8, 19, 29, 67, 121, and 206 μM with [^{15}N]Jd and 0, 9.8, 19, 29, 39, 57, and 94 μM with [^{15}N]JdD35N. Final concentrations of KaseR167A were 0, 15, 29, 43, 59, 73, and 104 μM with both [^{15}N]Jd and [^{15}N]JdD35N. All NMR spectra were recorded at 25 °C on a Bruker DRX 500 spectrometer operating at 500 MHz. The spectrometer was equipped with a 5 mm Bruker inverse triple-resonance probe with a triple-axis gradient coil (TXI). Pulses were calibrated using standard methods. Proton chemical shifts were referenced to external 3,3,3-(trimethylsilyl)propionate (TSP). ^{15}N chemical shifts were referenced indirectly relative to the TSP ^{1}H frequency (*49*). Two-dimensional ^{15}N−^{1}H HSQC NMR spectra employed the standard Bruker pulse sequence with sensitivity improvement and phase-sensitive echo/antiecho−TPPI gradient selection (*50*, *51*) (*invif3gpsi*) with 2K acquisition points for spectral width 6009.6 Hz in the ^{1}H dimension and 256 increments in t_1 for 1800 Hz in the ^{15}N dimension. H$^\alpha$ resonance assignments for [^{15}N]JdD35N were obtained using standard Bruker 2D pulse sequences for 2D ^{15}N−^{1}H HSQC-TOCSY (MLEV17 for homonuclear Hartman−Hahn mixing, phase sensitive using echo/antiecho−TPPI gradient selection) (*52*, *53*), 2D ^{15}N−^{1}H HSQC-NOESY (phase sensitive using echo/antiecho−TPPI gradient selection) (*52*, *53*), and 3D ^{15}N−^{1}H HSQC-NOESY [using sensitivity improvement, phase sensitive using States−TPPI (t_1) and echo/antiecho−TPPI gradient selection (t_2)] (*50*, *51*), which are *invietf3gpml* (35 ms spin lock), *invietf3gpno* (150 ms mixing time), and *noesiif3gpsi3d* (125 ms mixing time), respectively.

RESULTS

Properties of the D35N Mutant J-Domain. In purification, the behavior of JdD35N was indistinguishable from that for Jd (*32*), except that it eluted from the Bio-Rex 70 cation-exchange column at 0.34 M NaCl instead of 0.12 M NaCl, suggesting that it presents a more positively charged surface. According to circular dichroism spectra, the secondary structure content of JdD35N is identical to that for Jd (Figure 1a). JdD35N exhibits a 1 deg lower thermostability than Jd but remains well folded up to 65 °C (Figure 1b).

A shift in the conformation of the loop containing D35 could affect the function of the J-domain. Of the 58 H$^\alpha$ resonances that could be assigned in JdD35N at pH 6.7, only those for residues H33, R36, and the terminal residue E75 deviated by more than 0.1 ppm from the values for J(2−79) in PDB file 1BQZ (*54*) (Figure 1c). (A systematic deviation presumably arising from different referencing was removed by subtracting the average difference for all residues from the value for each residue.) On the basis of differences in the structure of DnaJ(2−79) and DnaJ(2−105), Prestegard and co-workers proposed that loop II−III has two preferred conformations that are associated with alternate tertiary arrangements of helix IV (*54*). A modest difference (0.04 ppm) was reported in the H$^\alpha$ chemical shift of H33 between J(2−79) and J(2−105), and no difference was reported for R36. However, the difference for H33 was the second largest difference in H$^\alpha$ chemical shift between the two structures. The much greater chemical shift difference at H33 between JdD35N and J(2−79) may be due to a strong preference for a single conformer of loop II−III in the mutant J-domain.

Energetics of Jd and JdD35N Binding to the R167A Mutant ATPase Domain. Binding of Jd and JdD35N to KaseR167A was investigated by isothermal titration calorimetry (Table 1). Results for Jd and JdD35N binding to wild-type Kase have been reported elsewhere (*33*). The uncertainties in N, K_A, and ΔH are from the fits. The propagated uncertainties in K_D, ΔG, and $T\Delta S$ are asymmetric. For K_D, the uncertainty is reported as a range. For ΔG and $T\Delta S$, the larger arm of uncertainty is reported. The global uncertainty in measurements from multiple experiments was found to be larger that the uncertainty in fitting, presumably

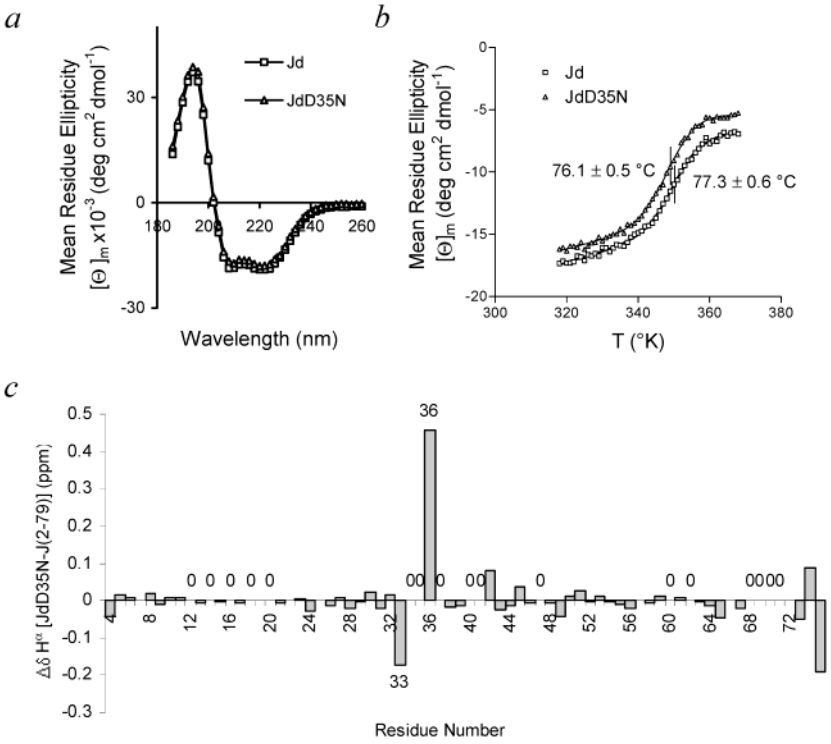

FIGURE 1: Structural consequences of the D35N mutation on Jd: (a) circular dichroism spectra of Jd and JdD35N; (b) thermal denaturation of Jd and JdD35N monitored by circular dichroism at 222 nm; (c) differences in the H^{α} chemical shift between JdD35N and DnaJ(2−79) (PDB: 1BQZ). H^{α} chemical shifts that could not be assigned at this pH are indicated by 0. Large H^{α} chemical shift differences at only two positions suggest a change in bias of the equilibrium between two favored conformations in loop II−III (*54*).

Table 1: Thermodynamics of Binding Wild-Type and Mutant Jd and Kase at 20 °C

	Jd-Kase[a]	JdD35N-Kase[a]	JdD35N-KaseR167A	Jd-KaseR167A
N	1.21 ± 0.05	1.04 ± 0.02	0.91 ± 0.02	0.67± 0.08
$K_A \times 10^{-3}$ (M^{-1})	50.8 ± 5.5	213 ± 28	229 ± 22	31.9 ± 3.5
K_D (μM)	17.8−22.1	4.1−5.4	4.0−4.8	28.2−35.3
ΔH (kcal)	0.32 ± 0.02	0.49 ± 0.02	0.63 ± 0.02	0.68 ± 0.09
ΔG (kcal)	−6.62 ± 0.07	−7.14 ± 0.08	−7.19 ± 0.06	−6.04 ± 0.07
$T\Delta S$ (kcal)	6.31 ± 0.08	7.63 ± 0.10	7.81 ± 0.07	6.72 ± 0.16

[a] From ref *33*.

due to variations in solution composition and pH. The average and standard deviations of fitted values for three experiments with Jd and Kase were as follows: $N = 1.14 \pm 0.35$, $K_A = 43500 \pm 6400$ M^{-1} (corresponding to $K_D = 23$ μM and range 20.0−27.0 μM), and $\Delta H = 0.41 \pm 0.25$ kcal mol^{-1} (*33*). Using these values, the calculated ΔG for Jd-Kase binding is -6.22 ± 0.09. For each of the protein pairs reported in the present study, the number of binding sites (N) deviates from 1.00 by less than the global uncertainty in Jd-Kase binding, and therefore N is most likely 1 for all pairs.

The interaction of D35 and R167 can be analyzed in terms of the double mutant cycle, which reveals free energy coupling between sites (*55*). The effect of R167A on binding depends on the status of D35. R167A has no effect on the free energy of JdD35N binding ($\Delta\Delta G_{R167A(D35N)} = \Delta G_{JdD35N-KaseR167A} - \Delta G_{JdD35N-Kase} = -0.04$), but it disfavors Jd binding ($\Delta\Delta G_{R167A} = \Delta G_{Jd-KaseR167A} - \Delta G_{Jd-Kase} = 0.27$). Thus, the free energy of interaction between D35 in Jd and R167 in Kase ($\Delta\Delta G_{int} = \Delta\Delta G_{R167A(D35N)} - \Delta\Delta G_{R167A}$) is −0.31 kcal/mol. Since this is more than twice as large as the global uncertainty in ΔG, the two residues have a small favorable interaction.

Correlation of Integrated Chemical Shift Perturbation with the Free Energy of Binding. $^1H-^{15}N$ HSQC NMR spectra were recorded for samples containing 40 μM [^{15}N]Jd or [^{15}N]JdD35N and increasing concentrations of Kase or KaseR167A. Cross-peaks from backbone amide groups of 44 residues could be resolved in spectra of both [^{15}N]Jd and [^{15}N]JdD35N over the entire range of the titration with Kase. Unresolved amide groups exchanged too rapidly with solvent, overlapped with other amide groups, or were severely broadened at high concentrations of Kase. Chemical shift perturbations ($\Delta\delta$) for the various protein combinations were approaching saturation at the highest Kase or KaseR167A concentration (Figure 2).

A change in the resonance frequency for a given nucleus indicates that the nucleus has moved into a different chemical environment. The observed frequency depends on the rate of exchange between bound and free states and on the difference in frequency induced by the two chemical environments. If the exchange is slow by comparison to the frequency difference, then the new frequency corresponds to only the bound state. If the exchange is fast, then the new frequency is the weighted average of frequencies corresponding to the bound and free states. Almost all of the chemical shift changes observed in [^{15}N]Jd or [^{15}N]JdD35N upon binding to Kase were in fast exchange, as indicated by the gradual movement of cross-peaks from one place to another in the spectrum, as the Kase concentration was increased. A few exceptions in Jd-Kase binding (Y6, Y54) were noted previously (*32*), and several additional amides (Y7, L10, S13, R19, K40, and K46) became too broad to monitor at high Kase concentrations in experiments with

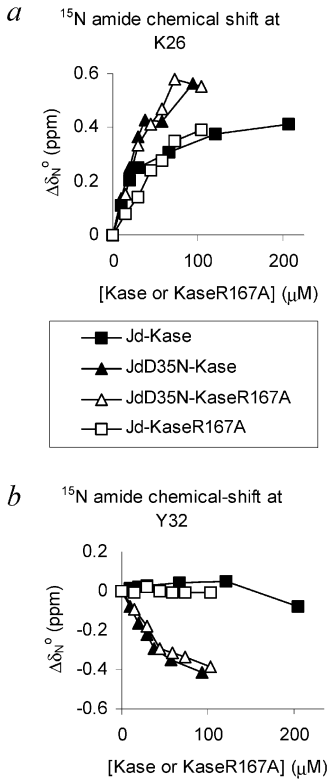

FIGURE 2: Binding of [^{15}N]Jd or [^{15}N]JdD35N to Kase or KaseR167A monitored by NMR chemical shift perturbation. ^{15}N chemical shift perturbations were saturable and differentially affected by the mutations.

[^{15}N]JdD35N. These amide groups are likely to be in intermediate to slow exchange due to an exceptionally large chemical shift change upon binding to Kase. All of these resonances were excluded from further analysis.

To compare chemical shift perturbations in fast exchange between different NMR samples, it is necessary to take into account the extent of binding. One way would be to compare spectra at very high Kase concentrations, where essentially all of the [^{15}N]Jd is bound. However, such an experiment would be difficult because T_2 relaxation in the [^{15}N]Jd-Kase complex (approximately 50 kDa) makes the resonances too broad. At lower Kase concentrations, the concentration of [^{15}N]Jd bound can be calculated by solving a quadratic expression for the K_D. In theory, the K_D could be determined by fitting the curve of chemical shift vs Kase concentration. However, in practice, it is difficult to get enough points for a good fit, especially at the two extremes. For this work, the K_D was determined by ITC. Once the fraction of [^{15}N]Jd or [^{15}N]JdD35N bound for each sample is known, one can compare profiles of chemical shift perturbation for samples having the same fraction bound. Alternatively, the profiles of chemical shift perturbations can be normalized to the same fraction bound, as will be described below.

To compare chemical shift perturbations for the various Jd-Kase pairs, a composite value for the chemical shift change in the ^{15}N and ^{1}H dimensions at each amide was calculated as follows: $\Delta\delta_c = [(\delta_{^1H})^2 + (0.17\delta_{^{15}N})^2]^{1/2}$. The factor of 0.17 accounts for the greater sensitivity of ^{15}N to perturbation. In a preliminary comparison of chemical shift perturbation profiles for [^{15}N]Jd-Kase and [^{15}N]JdD35N-Kase at the same fraction bound, it was clear that the $\Delta\delta_c$ were generally of larger magnitude and more broadly distributed in [^{15}N]JdD35N. Since the ITC results indicated that JdD35N binds with greater affinity than Jd to Kase, it seemed likely that the increases in chemical shift perturbations were due to the greater binding affinity. Thus, a quantitative comparison of chemical shift perturbations was undertaken.

The integrated composite chemical shift perturbations ($\sum\Delta\delta_c$) for the various Jd-Kase pairs were tested for a correlation with the free energies of binding. The $\sum\Delta\delta_c$ is the sum of the chemical shift perturbations at all 44 measured amide groups in [^{15}N]Jd or [^{15}N]JdD35N. Values of $\sum\Delta\delta_c$ were calculated from spectra for each Jd-Kase pair at approximately 38%, 50%, and 60% J-domain complexed. The three values of $\sum\Delta\delta_c$ for each protein pair were extrapolated to the value expected for 100% J-domain complexed ($\sum\Delta\delta_c^\circ$) and then treated as independent determinations of the same property. When analyzed by linear regression, $\sum\Delta\delta_c^\circ$ correlated well with free energy of binding (ΔG) obtained from ITC (Figure 3a). Essentially the same

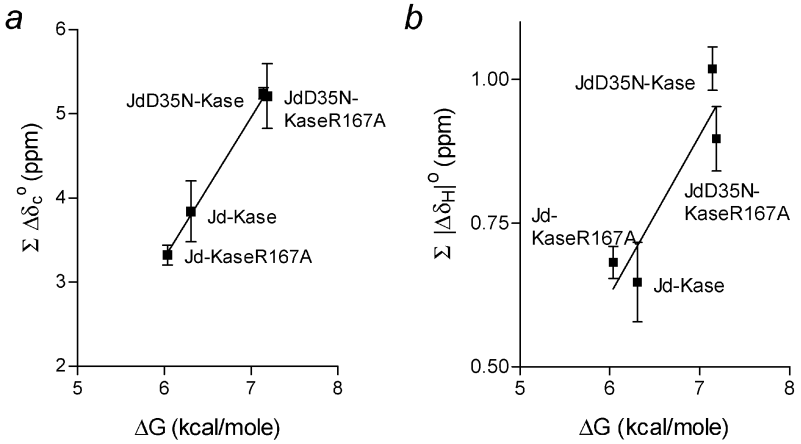

FIGURE 3: Correlation of chemical shift perturbation with the free energy of binding: (a) correlation using integrated composite chemical shift perturbations for all measured amides ($r^2 = 0.87$, $P < 0.0001$); (b) correlation using integrated ^{1}H chemical shift perturbations for amides in helix II ($r^2 = 0.69$, $P = 0.0008$). Each value of $\sum\Delta\delta_c^\circ$ or $\sum|\Delta\delta_H|^\circ$ is the average perturbation at 100% binding from determinations at three concentrations of Kase or KaseR167A. For each determination, the sum of $\Delta\delta_c$ or $|\Delta\delta_H|$ at 44 amides was divided by the fraction bound, calculated using the appropriate K_D from ITC. The fractions bound in the three samples for each pair of proteins were as follows: [^{15}N]Jd and Kase (29, 67, 121 μM), 0.33, 0.53, 0.67; [^{15}N]JdD35N and Kase (29, 39, 57 μM), 0.40, 0.46, 0.57; [^{15}N]JdD35N and KaseR167A (29, 43, 59 μM), 0.40, 0.50, 0.58; [^{15}N]Jd and KaseR167A (43, 73, 104 μM) 0.38, 0.51, 0.60.

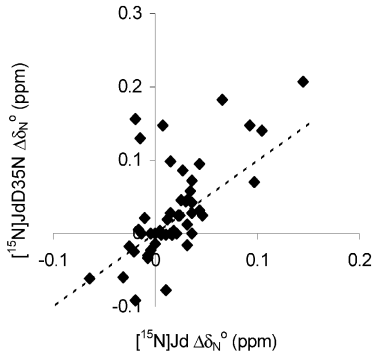

FIGURE 4: Plot of amide ^{15}N chemical shift perturbations in [^{15}N]-JdD35N vs amide ^{15}N chemical shift perturbations in [^{15}N]Jd. Chemical shift perturbations from the [^{15}N]JdD35N-Kase sample with 57% bound and the [^{15}N]Jd-Kase sample with 67% bound were divided by the fraction bound and then plotted against each other. The dashed line has a slope of 1, indicating equal perturbation for [^{15}N]JdD35N and [^{15}N]Jd. Since almost all of the significant $\Delta\delta_N°$ are larger for [^{15}N]JdD35N than for [^{15}N]Jd, it is unlikely that changes caused by D35N are due to the repositioning of an aromatic ring in the interface.

correlation was obtained when every fifth amide was eliminated from the set of 44 amides analyzed (data not shown), suggesting that the correlation does not strongly depend on the selection of amides.

A correlation of $\sum\Delta\delta_c°$ with ΔG in such a small number of points (corresponding to four protein pairs) might arise by chance if an aromatic ring in the binding site were responsible for many of the chemical shift perturbations. In this case, the direction of an individual chemical shift change would depend on the location of the resonant nucleus relative to the plane of the ring. If a mutation affects the relative position of the ring, then changes in $\Delta\delta_H$ or $\Delta\delta_N$ would be distributed both upfield and downfield. This possibility was investigated by comparing the ^{15}N chemical shift perturbation at each amide for 100% [^{15}N]JdD35N and 100% [^{15}N]Jd complexed (Figure 4). The distribution of points indicates that almost all of the perturbations are either more positive or more negative for [^{15}N]JdD35N than for [^{15}N]Jd. Since the direction of the chemical shift change upon binding to Kase was the same for both proteins, the correlation of $\sum\Delta\delta_c°$ with ΔG most likely arises from structural factors other than proximity to an aromatic ring, such as the length of hydrogen bonds.

Periodic NH Chemical Shift Perturbations in Helix II. Since amide−^{1}H chemical shifts seem to be most greatly influenced by hydrogen bond strength (*35*), profiles of ^{1}H chemical shift perturbation ($\Delta\delta_H$) were examined for evidence of changes in hydrogen-bonded structure upon binding of [^{15}N]Jd or [^{15}N]JdD35N to Kase or KaseR167A. To compare profiles for the various protein pairs, the $\Delta\delta_H$ for samples with approximately 60% J-domain bound were extrapolated to the expected value at 100% bound ($\Delta\delta_H°$). The profile of $\Delta\delta_H°$ in helix II (residues 19−30) reveals a periodicity that corresponds to the turns of an α helix (Figure 5). A periodic pattern of chemical shifts has been interpreted as helix bending in coiled coils (*56*, *57*) and in an isolated helix that contains a hydrophobic cluster (*58*). Thus, helix II bends upon binding to Kase. The upfield-shifted amide groups mark the convex side of the bend, where hydrogen bonds are longer. According to the three-dimensional structure, the convex side of the bend faces toward helix I.

Changes in hydrogen bond lengths associated with helix bending could be a mechanism underlying the correlation of chemical shift perturbation and binding energy. To test this possibility, the integrations of $\Delta\delta_H$ in helix II were tested for correlation with free energies of binding. For each protein pair, the integration of absolute values of $\Delta\delta_H$ for amides 19−30 was extrapolated to the value expected for 100% bound ($\sum|\Delta\delta_H|°$). The $\sum|\Delta\delta_H|°$ for helix II correlated with ΔG, although not as well as $\sum\Delta\delta_c°$ for the entire J-domain (Figure 3b).

Differences in Chemical Shift Perturbation Maps for [^{15}N]Jd and [^{15}N]JdD35N Binding to Kase and KaseR167A. The multiple determinations of $\Delta\delta_c$ provided a rigorous strategy for comparison of chemical shift perturbations in the various protein pairs. The three values of $\Delta\delta_c$ for each

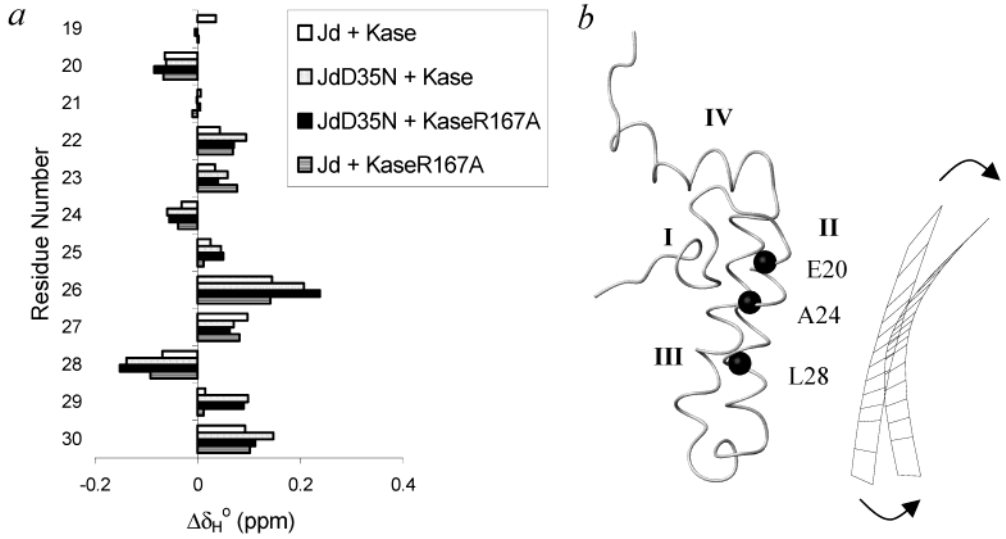

FIGURE 5: Bending of helix II upon binding to Kase. The ^{1}H chemical shift perturbations in helix II for [^{15}N]Jd-Kase at 67% bound, [^{15}N]JdD35N-Kase at 57% bound, [^{15}N]JdD35N-KaseR167A at 58% bound, and [^{15}N]Jd-KaseR167A at 60% bound were divided by the fraction bound in order to obtain $\Delta\delta_H°$. The periodicity of $\Delta\delta_H°$ coincides with turns in the helix. On the basis of predicted changes in hydrogen bond lengths, the three upfield-shifted amide groups (corresponding N atoms illustrated) would lie on the convex side of the bend. Panels illustrate the location and direction, not necessarily the magnitude, of the bend.

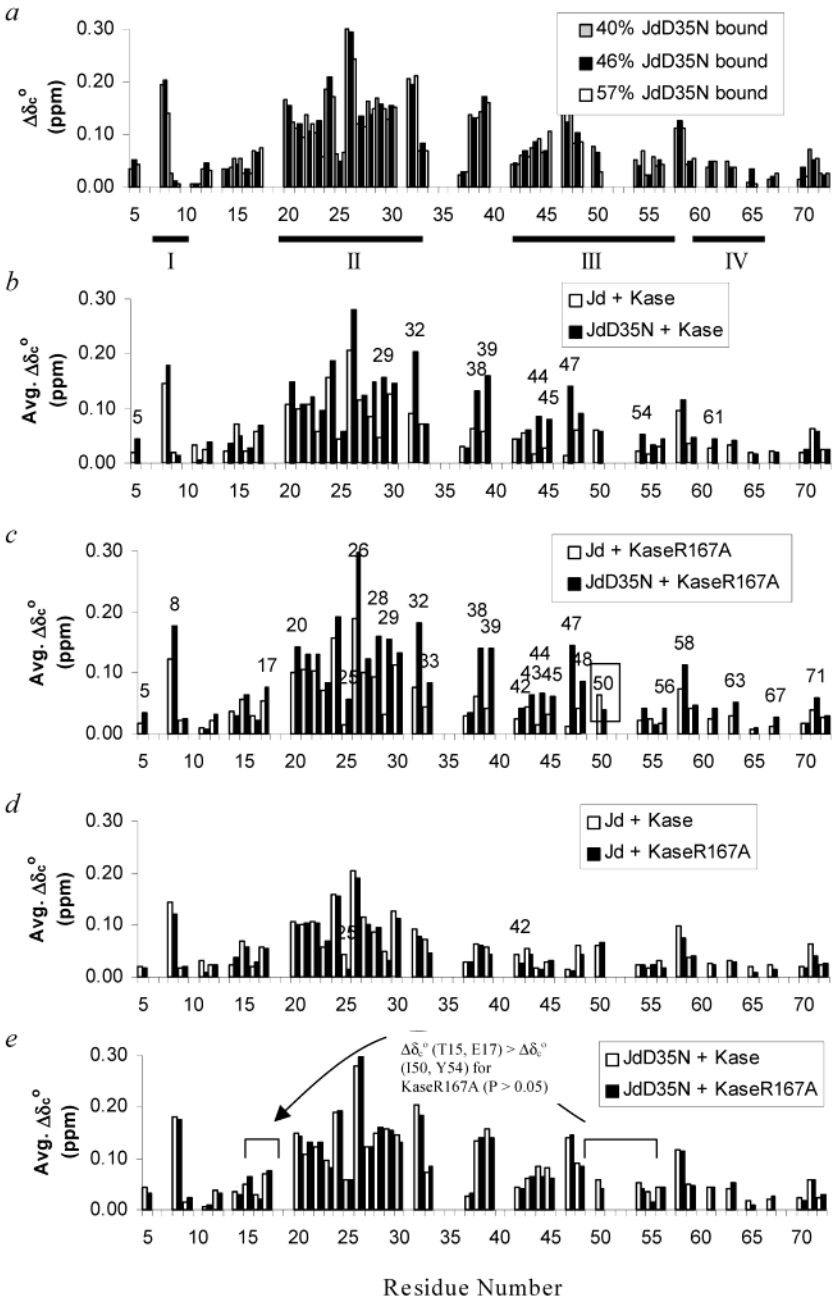

FIGURE 6: Effect of mutations on amide group chemical shift perturbations in [^{15}N]Jd and [^{15}N]JdD35N induced by Kase or KaseR167A. (a) Composite (^{1}H, ^{15}N) chemical shift perturbations for [^{15}N]JdD35N binding to Kase at the indicated levels of binding and then extrapolated to 100% binding. Bars indicated the locations of the four α helices. (b−e) Average of three composite (^{1}H, ^{15}N) chemical shift perturbations divided by the fraction bound in the sample. The fractions bound were as described in the legend for Figure 3. Residue numbers in the data labels indicate significant differences in the magnitude of perturbation between pairs ($P < 0.05$). Magnitudes of perturbation by Kase were significantly greater in [^{15}N]JdD35N than in [^{15}N]Jd for amides located mainly in the carboxy-terminal portion of helix II, loop II−III, and the amino-terminal portion of helix III. Magnitudes of perturbation by KaseR167A were significantly greater in [^{15}N]JdD35N than in [^{15}N]Jd for a broader distribution of amides, but the largest differences were in the region of loop II−III. Perturbation by KaseR167A was significantly lower in [^{15}N]JdD35N than in [^{15}N]Jd at one position (boxed). Perturbation by KaseR167A of [^{15}N]Jd was significantly lower than by Kase at two amides. Perturbation by KaseR167A and Kase of [^{15}N]JdD35N was not significantly different at any amide, but the relative perturbation at two amides in helix III was significantly lower than at two amides in loop I−II for [^{15}N]JdD35N with KaseR167A but not with Kase.

amide from spectra with approximately 38%, 50%, and 60% [^{15}N]Jd or [^{15}N]Jd D35N bound were extrapolated to the value expected for 100% bound ($\Delta\delta_c°$). The precision of the measurements and validity of the extrapolation are evident in the profile of [^{15}N]JdD35N with Kase (Figure 6a). The average standard deviations in 44 values of $\Delta\delta_c°$ were 0.017 ppm for [^{15}N]Jd-Kase, 0.012 ppm for [^{15}N]JdD35N-Kase, 0.013 ppm for [^{15}N]JdD35N-KaseR167A, and 0.008 ppm for [^{15}N]Jd-KaseR167A. Chemical shift perturbations at a given amide for the various protein pairs were compared in terms of the average $\Delta\delta_c°$, and the significance of differences was evaluated using the Student's *t*-test ($P < 0.05$). For mapping the distribution of perturbations, the average values of $\Delta\delta_c°$ were grouped into bins of $\Delta\delta_c° > 0.1$ ppm and $0.05 < \Delta\delta_c° < 0.1$ ppm and displayed on a diagram of the J-domain structure.

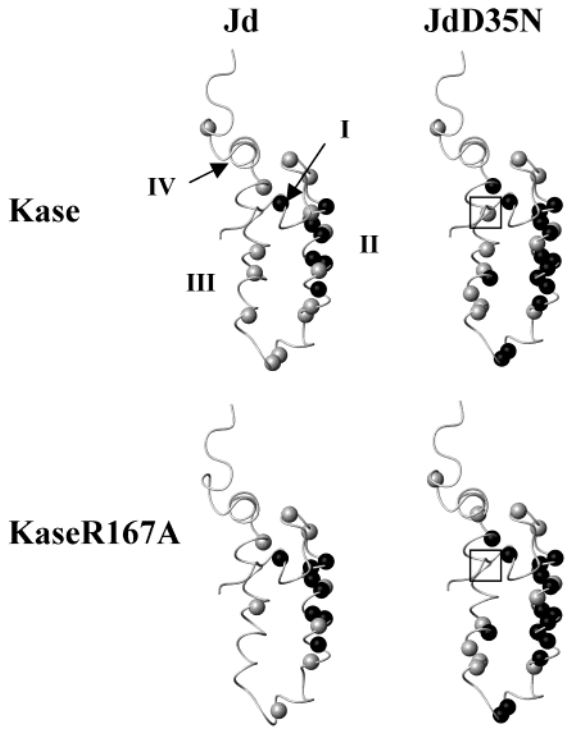

FIGURE 7: Locations in the J-domain structure of the most significant amide group chemical shift perturbations for the various protein pairs. Space-filled atoms indicate amide nitrogens with $\Delta\delta_c^\circ > 0.05$. Atoms in gray exhibit chemical shift perturbations in the range $1.0 > \Delta\delta_c^\circ > 0.05$. Atoms in black exhibit chemical shift perturbations of $\Delta\delta_c^\circ > 1.0$. Coordinates for the J-domain structure were from the PDB (1BQZ), and the figure was created in MOLMOL. D35N mainly increased $\Delta\delta_c^\circ$ at amides in loop II−III and helix III with Kase or KaseR167A, but it decreased $\Delta\delta_c^\circ$ at one amide in the C-terminal portion of helix III with KaseR167A (boxed).

The comparison of profiles for [^{15}N]JdD35N-Kase and [^{15}N]Jd-Kase indicates that D35N increased $\Delta\delta_c^\circ$ of amides mainly in the region surrounding loop II−III, where D35 is located (Figure 6b). Eight of 10 amides with significantly larger $\Delta\delta_c^\circ$ are located within this region (residues 29−54). With respect to the overall distribution of perturbed amides, D35N expanded the envelope of most strongly perturbed amides to include loop II−III and helix III (Figure 7). Four of 15 amides with $\Delta\delta_c^\circ$ greater than 0.1 ppm are located in loop II−III or helix III, whereas in [^{15}N]Jd-Kase, all of the seven amides with $\Delta\delta_c^\circ$ of this magnitude are located in helix I or II.

The comparison of profiles for [^{15}N]JdD35N-KaseR167A and [^{15}N]Jd-KaseR167A indicates that D35N increased $\Delta\delta_c^\circ$ for amides in most regions of the molecule, but the largest increases were in the region surrounding loop II−III (Figure 6c). D35N decreased $\Delta\delta_c^\circ$ at one amide (I50). As observed in experiments with Kase, D35N expanded the envelope of most strongly perturbed amides to include loop II−III and helix III (Figure 7). However, perturbation at two amides (I50 and Y54) in the C-terminal portion of helix III dropped below 0.05 ppm.

The comparison of profiles for [^{15}N]Jd-Kase and [^{15}N]Jd-KaseR167A indicates that R167A caused a small decrease in chemical shift perturbations for [^{15}N]Jd (Figure 6d). The $\Delta\delta_c^\circ$ was significantly reduced for one amide in helix II (Y25) and one amide in helix III (E41). In [^{15}N]Jd-KaseR167A, the envelope of most strongly perturbed amides was slightly more focused on helix II (Figure 7). The $\Delta\delta_c^\circ$ at five amides (H33, G39, A43, K48, and H71) dropped below 0.05 ppm. Four of these amides are located in the region surrounding loop II−III.

The comparison of profiles for [^{15}N]JdD35N-Kase and ^{15}N]JdD35N-KaseR167A indicates that R167A has a very small effect on perturbations of [^{15}N]JdD35N (Figure 6e). There were no significant differences in perturbation between the protein pairs. However, distinct interactions of [^{15}N]-JdD35N with KaseR167A and Kase were evident in the relative perturbation of amides in loop I−II (T15 and E17) and in the carboxy-terminal half of helix III (I50 and Y54). In [^{15}N]JdD35N-KaseR167A, the $\Delta\delta_c^\circ$ at T15 and E17 were significantly larger than the $\Delta\delta_c^\circ$ at I50 and Y54, whereas in [^{15}N]JdD35N-Kase, the $\Delta\delta_c^\circ$ at these four amides were indistinguishable.

DISCUSSION

The physical basis for an allele-specific genetic interaction was analyzed in order to reveal essential features in the interaction of the DnaJ J-domain with the DnaK ATPase domain. Work from several laboratories has shown that the role of the J-domain is to trigger ATP hydrolysis in DnaK, resulting in the capture a DnaJ-bound client protein by the DnaK peptide-binding domain (*4*, *5*, *18*, *33*, *59*, *60*). Initial studies found that DnaJ(D35N) had lost the ability to bind to DnaK (*16*). It is now clear that the D35N mutant J-domain retains the ability to bind to the DnaK ATPase domain and that the D35N mutation specifically blocks the mechanism that triggers ATP hydrolysis and protein capture (*33*). Several observations suggest that the DnaK ATPase domain contains the J-domain-binding site. (i) NMR signal perturbations in [^{15}N]Jd were nearly identical whether caused by Kase or full-length DnaK (*32*), (ii) R167A replaces a residue in an acidic groove on the DnaK ATPase domain (*16*), and (iii) rationally designed mutations that affect residues in the acidic groove disrupted DnaJ−DnaK functional interaction (*20*). Nevertheless, mutations affecting residues in the ATPase domain could disrupt interaction with the peptide-binding domain and therefore indirectly disrupt DnaJ−DnaK interaction because DnaJ also binds to the DnaK peptide-binding domain (*18*). Studies on the physical interaction of the wild-type and mutant J-domain and ATPase domain could shed light on the mechanism by which the J-domain stimulates DnaK activities and support or refute the hypothesis that the acidic groove contains the J-domain-binding site.

NMR chemical shift perturbation mapping reveals a distorted mode of [^{15}N]JdD35N binding to Kase. The more intense and more broadly distributed perturbations could reflect the strengthening and recruitment of intermolecular bonds within and beyond the wild-type binding interface in helix II and adjacent HPD tripeptide. This interpretation is consistent with the increased binding affinity observed for JdD35N binding to Kase (*33*). Alternatively, the increased perturbations could reflect a more significant conformational change in D35N upon binding to Kase. As has been discussed, it is not possible to distinguish perturbations caused by direct contacts across the intermolecular interface from perturbations caused by a conformational change associated with binding (*40*). In the present work, we find evidence for a conformational change, but the recruitment

of new intermolecular bonds may also contribute to the distorted mode of [^{15}N]JdD35N binding to Kase.

The perturbation map for [^{15}N]Jd-Kase indicated the interface to be centered on K26 in helix II and extending over the conserved HPD tripeptide in loop II−III (*32*). The functional importance of K26 has been confirmed by results from alanine scanning mutagenesis (*61*). Enhanced perturbations in loop II−III and helix III of [^{15}N]JdD35N could indicate the expansion of the binding interface, which would be consistent with the higher affinity of JdD35N for Kase. Since the ΔG of protein−protein binding scales linearly with buried hydrophobic surface area (*62*), one could postulate that $\sum\Delta\delta_c^\circ$ scales linearly with ΔG because $\sum\Delta\delta_c^\circ$ indicates the size of the interface. However, the conventional interpretation of chemical shift perturbation does not predict a general increase in the magnitudes of perturbations with increase in affinity, and this also was observed for [^{15}N]-JdD35N binding to Kase.

A conformational change in the J-domain is necessary to explain the NMR chemical shift perturbation data. A mutation could produce a local increase in the magnitude of chemical shift perturbations if there was a local change in the structure of the interface, such as a change in the position or orientation of an aromatic ring. However, in the present case, almost all of the resonances that were strongly perturbed by Kase in [^{15}N]Jd were perturbed in the same direction and to a greater extent by Kase in [^{15}N]JdD35N. To account for this observation, we regard the structure of Jd or JdD35N as a dynamic ensemble of conformations. Thus, the general increase in magnitude of chemical shift changes with increase in affinity is due to smaller conformational fluctuations in the bound state.

Large-scale J-domain conformational fluctuations could be sampled by the NMR-averaged chemical shift perturbations. The largest $\Delta\delta_H^\circ$ sets the slow limit on the exchange rate between bound and free states of the J-domain, and the largest $\Delta\delta_H^\circ$ was approximately 0.25 ppm, corresponding to 125 Hz. In order for this resonance to be in the fast-exchange regime, it must exchange at a rate not less than 10 times 125 Hz, which corresponds to a relaxation time of up to 800 μs. Many proteins are known to exchange between folded and unfolded states on considerably shorter time scales (*63*). Thus the ensemble of free and Kase-bound J-domain conformations that contribute to the average chemical shifts may include conformations that are significantly different from each other.

This appears to be the first study finding a correlation between binding affinity and NMR chemical shift perturbation in a protein−protein interaction, although theory and experiment predict such a relationship. The notion that binding is energetically coupled to the structure of the binding protein underpins the theory of induced fit by enzymes to substrates (*64*−*66*), and the coupling of protein folding and binding has been well documented in DNA-binding proteins (*67*).

Productive interaction of the J-domain and DnaK ATPase domain may require an induced fit conformational change in the J-domain that involves loop II−III. Zsyperski et al. proposed that conformational flexibility in loop II−III and the amino-terminal portion of helix III would allow this region to undergo an induced fit upon binding to DnaK (*23*). Huang et al. showed that the presence of the Gly/Phe-rich domain in DnaJ(2−105) is associated with a change in the bias of the conformational equilibrium in loop II−III (*54*), and they have suggested that the J-domain uses these dynamics to coordinate interactions with the ATPase domain and peptide-binding domain of DnaK (*54*, *68*). The present results suggest that the D35N mutant J-domain is overstabilized in the conformation induced by binding to Kase. The absence of large chemical shift perturbations in loop II−III and helix III of [^{15}N]Jd indicates that Kase binding does not induce conformations with substantial differences in loop II−III and helix III. In contrast, numerous large perturbations were induced in these regions of [^{15}N]JdD35N. Since JdD35N binds with higher affinity than Jd to Kase, the mutant J-domain might more easily undergo an induced fit conformational change. The wild-type J-domain may also undergo this conformational change, but only when fused to the Gly/Phe-rich region or when coupled to a DnaK conformational change.

A requirement for dynamics is consistent with a catalytic role for the J-domain, in which it lowers the high-energy barrier (*69*) for conformational change in DnaK (*33*). Dynamic features are thought to be an essential property of many enzymes (*70*), and dynamic flexibility in loop II−III has been implicated in J-domain function (*54*, *68*, *71*, *72*). The J-domain could stabilize the transition state rather than either the "closed" or "open" conformation of DnaK. A flexible J-domain might facilitate the interaction with DnaK as it crosses a high-energy conformational barrier. In contrast, a strong bias of the loop II−III conformation caused by D35N could favor binding to one of the equilibrium states of DnaK, which would account for both the increase in affinity and loss of function.

Bending of helix II accompanies the induced fit conformational change by the J-domain. The periodic pattern of ^{1}H chemical shift perturbations indicates that helix II bends when Jd binds to Kase. Helix II bending appears to be greater in JdD35N, and therefore helix II bending could be part of the change in the overall conformational ensemble that accounts for the correlation of $\sum\Delta\delta_c^\circ$ with ΔG. NMR studies on the structure and dynamics of J-domain-containing molecules indicate that helices I, II, and the carboxy-terminal portion of helix III form a stable core (*71*), but helix II is distinguished by motions on longer time scales than the rest of the molecule. On the basis of ^{15}N-relaxation measurements, the model-free description for amide group motions in helix II of DnaJ(2−79) required two components on the picosecond to nanosecond time scale, whereas the description for most other amide groups required only one component (*68*). Similar measurements on the J-domain of DnaJ(2−105) found evidence for motion on the 1 μs to 1 ms time scale at numerous positions in the J-domain, and ^{13}C-relaxation studies indicated that the J-domain exhibits anisotropic components of motion that could involve helical segments (*68*). As suggested by Huang et al., J-domain conformational fluctuations could play a role in coupling the ATPase with peptide binding in DnaK (*68*). D35N could overstabilize a subset of J-domain conformations and therefore eliminate a conformational fluctuation, such as helix II bending, that couples ATP hydrolysis with a conformational change in DnaK.

The R167A mutation in DnaK may suppress the defect in DnaJ(D35N) by disfavoring the induced fit conformational

change. Helix II bending was reduced (Figure 3), the effect of D35N was reversed at one amide in helix III (Figure 6c and 7), and the magnitude of two perturbations in helix III was reduced relative to loop I−II (Figure 6e). These are subtle changes by comparison to the effect of D35N, but the phenotype of R167A is also relatively weak. DnaK(R167A) reversed the DnaJ(D35N)−DnaK binding defect in vitro, but it only partially suppressed the defect of DnaJ(D35N) in vivo (*16*). [DnaK(R167A) was created by Suh et al. to explore the side-chain requirements of position 167, which was identified as important for interaction with DnaJ(D35N) by the genetic selection of DnaK(R167H). KaseR167A was chosen for study in this work in order to avoid complications from ionization of the histidine side chain.] In view of the proposed requirement for dynamic interaction between the J-domain and ATPase domain, it is possible that J-domain contact with R167 normally causes strain in the J-domain that can be relieved by a conformational change in DnaK. The notion that D35 and R167 together contribute to strain in the J-domain is supported by their favorable interaction energy. D35N might allow this contact without strain in the J-domain, resulting in the failure of JdD35N to stimulate the conformational change in DnaK (*33*). Elimination of the contact by R167A might restore the strain in the J-domain and therefore also restore stimulation of the conformational change.

A putative contact of R167 with the J-domain could be important for inducing the conformational change in the wild-type J-domain. KaseR167A binds Jd with reduced affinity. Nevertheless, reductions in chemical shift perturbations for [^{15}N]Jd with KaseR167A were subtle, and the most significantly perturbed region remained focused on helix II. If most of the induced fit conformational change in the J-domain normally is coupled to a DnaK conformational change, then the induced conformation may be poorly represented in the chemical shift perturbations of [^{15}N]Jd. Nevertheless, the conformational change could be disrupted by loss of contact with R167. The disruption of unproductive contacts is a recurrent theme in allele-specific genetic interactions. It seems to be easier to find mutations that disrupt unproductive (although nativelike) contacts than to find mutations that restore wild-type contact at the site of the original mutation (*73*−*75*).

An increase in binding affinity creates a mechanism for alternative pathways for suppression of a defective protein−protein interaction. The suppressor mutation can disrupt contacts in order to restore a functional interaction without necessarily reversing the effects of the first mutation. The notion that a suppressor is more likely to disrupt a counterproductive contact than to restore a productive contact was articulated by MacNab and co-workers for FliM suppressors of CheY mutations (*74*). In that case, the disrupted contact shifted the bias of the flagellar motor toward clockwise rotation. In the case of the DnaJ−DnaK interaction, R167A may restore function, not by correcting the contact near D35N but rather by disrupting another contact that restores a functional mode of binding. Gross and co-workers had originally sought to obtain suppressors of a different J-domain mutant, DnaJ(H33Q), but failed to find any such suppressor mutations in DnaK. Suppression of H33Q may have been much more difficult because it lowers the binding affinity.

ACKNOWLEDGMENT

Thanks to N. K. Steede for protein purification, to K. Maskos and the Coordinated Instrumentation Facility for assistance with NMR spectroscopy, and to the New Orleans Protein Folding Intergroup for discussion. Thanks also to two reviewers who made many useful suggestions for improving this paper.

REFERENCES

1. Ang, D., Liberek, K., Skowyra, D., Zylicz, M., and Georgopoulos, C. (1991) *J. Biol. Chem. 266*, 24233−24236.
2. Mayer, M. P., and Bukau, B. (1998) *Biol. Chem. 379*, 261−268.
3. Liberek, K., Marszalek, J., Ang, D., Georgopoulos, C., and Zylicz, M. (1991) *Proc. Natl. Acad. Sci. U.S.A. 88*, 2874−2878.
4. Liberek, K., Wall, D., and Georgopoulos, C. (1995) *Proc. Natl. Acad. Sci. U.S.A. 92*, 6224−6228.
5. Gamer, J., Bujard, H., and Bukau, B. (1992) *Cell 69*, 833−842.
6. Schroder, H., Langer, T., Hartl, F. U., and Bukau, B. (1993) *EMBO J. 12*, 4137−4144.
7. Greener, T., Grant, B., Zhang, Y., Wu, X., Greene, L. E., Hirsh, D., and Eisenberg, E. (2001) *Nat. Cell Biol. 3*, 215−219.
8. Hoff, K. G., Silberg, J. J., and Vickery, L. E. (2000) *Proc. Natl. Acad. Sci. U.S.A. 97*, 7790−7795.
9. Misselwitz, B., Staeck, O., and Rapoport, T. A. (1998) *Mol. Cell 2*, 593−603.
10. Flaherty, K. M., Delucaflaherty, C., and McKay, D. B. (1990) *Nature 346*, 623−628.
11. Harrison, C. J., HayerHartl, M., DiLiberto, M., Hartl, F. U., and Kuriyan, J. (1997) *Science 276*, 431−435.
12. Zhu, X. T., Zhao, X., Burkholder, W. F., Gragerov, A., Ogata, C. M., Gottesman, M. E., and Hendrickson, W. A. (1996) *Science 272*, 1606−1614.
13. Schmid, D., Baici, A., Gehring, H., and Christen, P. (1994) *Science 263*, 971−973.
14. Jordan, R., and McMacken, R. (1995) *J. Biol. Chem. 270*, 4563−4569.
15. Sousa, M. C., and McKay, D. B. (1998) *Biochemistry 37*, 15392−15399.
16. Suh, W. C., Burkholder, W. F., Lu, C. Z., Zhao, X., Gottesman, M. E., and Gross, C. A. (1998) *Proc. Natl. Acad. Sci. U.S.A. 95*, 15223−15228.
17. Montgomery, D. L., Morimoto, R. I., and Gierasch, L. M. (1999) *J. Mol. Biol. 286*, 915−932.
18. Mayer, M. P., Laufen, T., Paal, K., McCarty, J. S., and Bukau, B. (1999) *J. Mol. Biol. 289*, 1131−1144.
19. Davis, J. E., Voisine, C., and Craig, E. A. (1999) *Proc. Natl. Acad. Sci. U.S.A. 96*, 9269−9276.
20. Gassler, C. S., Buchberger, A., Laufen, T., Mayer, M. P., Schroder, H., Valencia, A., and Bukau, B. (1998) *Proc. Natl. Acad. Sci. U.S.A. 95*, 15229−15234.
21. Han, W., and Christen, P. (2001) *FEBS Lett. 497*, 55−58.
22. Bork, P., Sander, C., Valencia, A., and Bukau, B. (1992) *Trends Biochem. Sci. 17*, 129.
23. Szyperski, T., Pellecchia, M., Wall, D., Georgopoulos, C., and Wuthrich, K. (1994) *Proc. Natl. Acad. Sci. U.S.A. 91*, 11343−11347.
24. Hill, R. B., Flanagan, J. M., and Prestegard, J. H. (1995) *Biochemistry 34*, 5587−5596.
25. Qian, Y. Q., Patel, D., Hartl, F. U., and McColl, D. J. (1996) *J. Mol. Biol. 260*, 224−235.
26. Cupp-Vickery, J. R., and Vickery, L. E. (2000) *J. Mol. Biol. 304*, 835−845.
27. Berjanskii, M. V., Riley, M. I., Xie, A., Semenchenko, V., Folk, W. R., and Van Doren, S. R. (2000) *J. Biol. Chem. 275*, 36094−36103.
28. Kim, H. Y., Ahn, B. Y., and Cho, Y. (2001) *EMBO J. 20*, 295−304.
29. Sawai, E. T., Rasmussen, G., and Butel, J. S. (1994) *Virus Res. 31*, 367−378.
30. Fewell, S. W., Pipas, J. M., and Brodsky, J. L. (2002) *Proc. Natl. Acad. Sci. U.S.A. 99*, 2002−2007.
31. Scidmore, M. A., Okamura, H. H., and Rose, M. D. (1993) *Mol. Biol. Cell 4*, 1145−1159.
32. Greene, M. K., Maskos, K., and Landry, S. J. (1998) *Proc. Natl. Acad. Sci. U.S.A. 95*, 6108−6113.

33. Wittung-Stafshede, P., Guidry, J., Horne, B. E., and Landry, S. J. (2003) *Biochemistry 42*, 4937−4944.
34. Wagner, G., Pardi, A., and Wuthrich, K. (1983) *J. Am. Chem. Soc. 105*, 5948−5949.
35. Wishart, D. S., Sykes, B. D., and Richards, F. M. (1991) *J. Mol. Biol. 222*, 311−333.
36. Xu, X. P., and Case, D. A. (2002) *Biopolymers 65*, 408−423.
37. Kuhlmann, U. C., Pommer, A. J., Moore, G. R., James, R., and Kleanthous, C. (2000) *J. Mol. Biol. 301*, 1163−1178.
38. Welch, M., Chinardet, N., Mourey, L., Birck, C., and Samama, J. P. (1998) *Nat. Struct. Biol. 5*, 25−29.
39. Ding, W., Huang, X., Yang, X., Dunn, J. J., Luft, B. J., Koide, S., and Lawson, C. L. (2000) *J. Mol. Biol. 302*, 1153−1164.
40. Zuiderweg, E. R. (2002) *Biochemistry 41*, 1−7.
41. Pellecchia, M., Montgomery, D. L., Stevens, S. Y., Van der Kooi, C. W., Feng, H. P., Gierasch, L. M., and Zuiderweg, E. R. (2000) *Nat. Struct. Biol. 7*, 298−303.
42. Penkett, C. J., Dobson, C. M., Smith, L. J., Bright, J. R., Pickford, A. R., Campbell, I. D., and Potts, J. R. (2000) *Biochemistry 39*, 2887−2893.
43. Stevens, S. Y., Sanker, S., Kent, C., and Zuiderweg, E. R. (2001) *Nat. Struct. Biol. 8*, 947−952.
44. Ubbink, M., and Bendall, D. S. (1997) *Biochemistry 36*, 6326−6335.
45. Bergkvist, A., Ejdeback, M., Ubbink, M., and Karlsson, B. G. (2001) *Protein Sci. 10*, 2623−2626.
46. Ojennus, D. D., Fleissner, M. R., and Wuttke, D. S. (2001) *Protein Sci. 10*, 2162−2175.
47. Baber, J. L., Levens, D., Libutti, D., and Tjandra, N. (2000) *Biochemistry 39*, 6022−6032.
48. Pace, C. N., Hebert, E. J., Shaw, K. L., Schell, D., Both, V., Krajcikova, D., Sevcik, J., Wilson, K. S., Dauter, Z., Hartley, R. W., and Grimsley, G. R. (1998) *J. Mol. Biol. 279*, 271−286.
49. Markley, J. L., Bax, A., Arata, Y., Hilbers, C. W., Kaptein, R., Sykes, B. D., Wright, P. E., and Wuthrich, K. (1998) *J. Mol. Biol. 280*, 933−952.
50. Palmer, A. G., Cavanagh, J., Wright, P. E., and Rance, M. (1991) *J. Magn. Reson. 93*, 151−170.
51. Kay, L. E., Keifer, P., and Saarinen, T. (1992) *J. Am. Chem. Soc. 114*, 10663−10665.
52. Gronenborn, A. M., Bax, A., Wingfield, P. T., and Clore, G. M. (1989) *FEBS Lett. 243*, 93−98.
53. Norwood, T. J., Boyd, J., Heritage, J. E., Soffe, N., and Campbell, I. D. (1990) *J. Magn. Reson. 87*, 488−501.
54. Huang, K., Flanagan, J. M., and Prestegard, J. H. (1999) *Protein Sci. 8*, 203−214.
55. Horovitz, A. (1996) *Folding Des. 1*, R121−R126.
56. Goodman, E. M., and Kim, P. S. (1991) *Biochemistry 30*, 11615−11620.
57. Zhou, N. E., Zhu, B. Y., Sykes, B. D., and Hodges, R. S. (1992) *J. Am. Chem. Soc. 114*, 4320−4326.
58. Wiltscheck, R., Kammerer, R. A., Dames, S. A., Schulthess, T., Blommers, M. J., Engel, J., and Alexandrescu, A. T. (1997) *Protein Sci. 6*, 1734−1745.
59. Liberek, K., Marszalek, J., Ang, D., Georgopoulos, C., and Zylicz, M. (1991) *Proc. Natl. Acad. Sci. U.S.A. 88*, 2874−2878.
60. Karzai, A. W., and McMacken, R. (1996) *J. Biol. Chem. 271*, 11236−11246.
61. Genevaux, P., Schwager, F., Georgopoulos, C., and Kelley, W. L. (2002) *Genetics 162*, 1045−1053.
62. Janin, J., and Chothia, C. (1990) *J. Biol. Chem. 265*, 16027−16030.
63. Myers, J. K., and Oas, T. G. (2002) *Annu. Rev. Biochem. 71*, 783−815.
64. Koshland, D. E. (1958) *Proc. Natl. Acad. Sci. U.S.A. 44*, 98−104.
65. Jencks, W. P. (1975) *Adv. Enzymol. 43*, 219−410.
66. Narlikar, G. J., and Herschlag, D. (1998) *Biochemistry 37*, 9902−9911.
67. Spolar, R. S., and Record, M. T. (1994) *Science 263*, 777−784.
68. Huang, K., Ghose, R., Flanagan, J. M., and Prestegard, J. H. (1999) *Biochemistry 38*, 10567−10577.
69. Slepenkov, S. V., and Witt, S. N. (1998) *Biochemistry 37*, 16749−16756.
70. Hammes, G. G. (2002) *Biochemistry 41*, 8221−8228.
71. Pellecchia, M., Szyperski, T., Wall, D., Georgopoulos, C., and Wuthrich, K. (1996) *J. Mol. Biol. 260*, 236−250.
72. Berjanskii, M., Riley, M., and Van Doren, S. (2002) *J. Mol. Biol. 321*, 503.
73. Roman, S. J., Meyers, M., Volz, K., and Matsumura, P. (1992) *J. Bacteriol. 174*, 6247−6255.
74. Sockett, H., Yamaguchi, S., Kihara, M., Irikura, V. M., and Macnab, R. M. (1992) *J. Bacteriol. 174*, 793−806.
75. Richardson, A., vanderVies, S. M., Keppel, F., Taher, A., Landry, S. J., and Georgopoulos, C. (1999) *J. Biol. Chem. 274*, 52−58.

BI027070Y